Differential Sputter Yield Measurements of Single- and Multi-Element Targets due to Ion Beam Bombardment

A. Yalin, B. Rubin, J. Topper, and C. Farnell, Department of Mechanical Engineering, Colorado State University, Fort Collins, CO

ABSTRACT

Detailed knowledge of differential sputter yield profiles could aid in the optimization of coating processes based on ion beam etching. In this contribution an experimental setup and demonstrative results for measurement of differential sputter yield profiles (i.e., angular profiles of ejected particles) is presented. The facility employs a four-grid ion source to provide an approximately mono-energetic and collimated beam. Sputter yields are measured using a quartz crystal microbalance (QCM) deposition monitor. Total sputter yields (found by integrating the differential profiles) are validated against weight loss measurements and published values. The measured profiles are fit with Modified Zhang expressions to compactly describe the results using two fit parameters. Finally, demonstrative modeling that uses the ion beam conditions and differential sputter yield profiles to model and optimize placement of targets and substrates in coating processes is presented.

INTRODUCTION

The process in which atoms, molecules, clusters, or ions are ejected from the surface of a material due to bombarding incident ions is called ion sputtering [1]. Details of the sputtering process are of interest from both theoretical and applied viewpoints. Modeling of deposition requires knowledge of the differential (angular) sputter yields ($y(\alpha,\varphi)$) in order to track the trajectories of sputtered particles. Total and differential sputter yield profiles have been measured with a multitude of techniques, e.g., weight loss, collector plates, mass spectrometry, quartz crystal microbalance, Rutherford backscattering, radioactive tracers, and cavity ring-down spectroscopy.

In this contribution the quartz crystal microbalance (QCM) based experimental system for high sensitivity differential sputter yield measurements is described. This measurement approach uses a combination of weight loss and QCM deposition sensor [2-4]. In Section II, the experimental apparatus is explained. Section III includes a description of the measurement and data analysis procedures. Section IV contains results of the testing performed to validate the sensitivity and the accuracy of the experimental system. The results include total and differential sputter yields of gold under bombardment by xenon ions at ion energies range of 30-350 eV and at incidence angles 0-67.5 degrees. Section V shows an example of the sputter deposition modeling performed at this facility. Conclusions are given in Section VI.

EXPERIMENTAL APPARATUS

Description of Sputter Measurement System

A quartz crystal microbalance (QCM) deposition monitor is used to measure the differential sputter yields, which are then used to calculate the total sputter yield. Total sputter yield measurements are also performed using a weight loss approach. The scheme of the experimental apparatus is shown in Figure 1. The ion source and QCM are housed within a 0.125 m^3 stainless steel vacuum chamber (43 cm ID x 76 cm long main section), equipped with a 1500 liter/s CTI-8 cryogenic pump. The chamber base pressure is 4×10^{-7} Torr giving a working pressure of approximately 0.4 to 1×10^{-4} Torr. Target contamination effects in the vacuum chamber are estimated to be negligible, since for typical conditions the flux of ions incident on the target is approximately 100 times higher than the flux of nitrogen (the major contaminant) to the target [3]. A four-grid DC ion source has been specially designed for low energy operation. A rotatable target-mount is positioned 23 cm downstream of the ion source. Both QCM and target rotation are performed using high-precision stepper motors. A personal computer with LabView is used for controlling the QCM and target rotation and for data logging.

QCM Sensor and Temperature Control

In deposition mode, the QCM allows determination of differential sputter yields through measurement of mass accumulation (of sputtered particles) on its surface. For condensable components, sticking coefficients are assumed to be unity. Note that sticking coefficients for "new layers" and very thin layers (on the order of several angstroms) may be less than unity, but once a sufficient thickness of a given material has accumulated, sticking coefficients for condensables are generally unity [5]. For multi-component materials, such as BN, the sputtered particles may consist of a mix of condensable and non-condensable components.

The crystal signal comes from a Sigma Instruments SQC-339 Deposition Controller that reads the crystal frequency to 0.001 Hz and uses an RC-cut quartz crystal as opposed to the more conventional AC-cut crystal. The RC-cut crystal manufactured by Tangidyne Corporation is very accurate for

 505/856-7188

52nd Annual Technical Conference Proceedings, Santa Clara, CA, May 9–14, 2009 ISSN 0737-5921

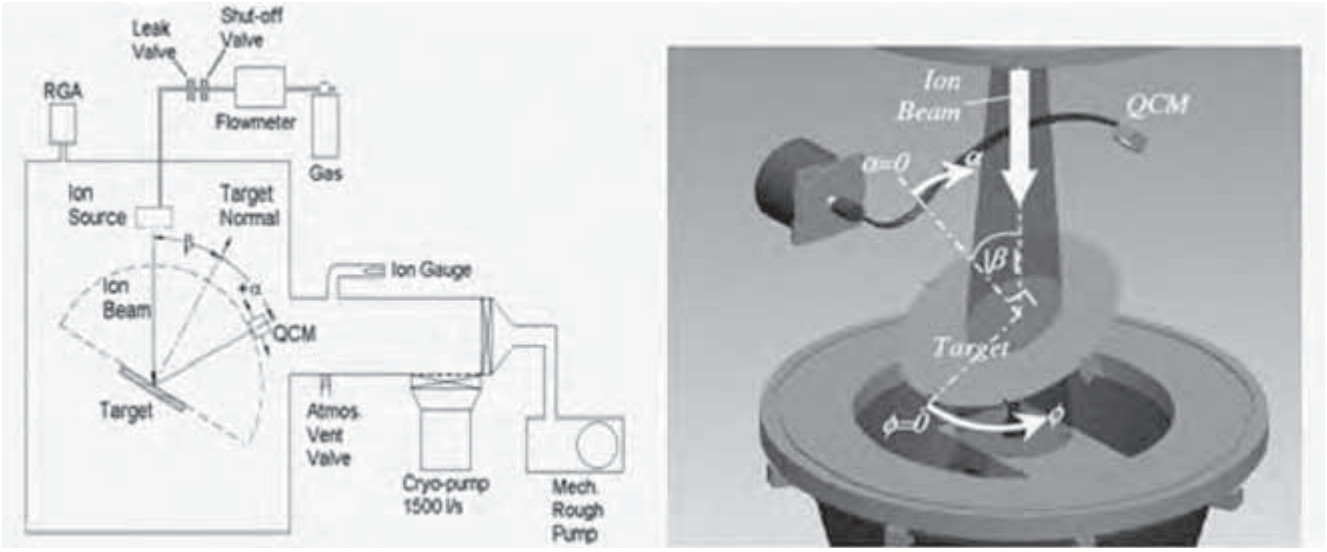

Figure 1: Schematic diagram of experimental set-up.

deposition of thin films. For most materials of interest, the RC-cut QCM enables measurement of differential sputter yield at ion energies as low as 30-60 eV.

Since quartz crystal resonance frequency is extremely sensitive to temperature variation, a cooling water loop controller with precision better than ±0.01°C is used [4]. A feedback system is used to combat the varying heat fluxes as the QCM position is moved. Temperature stability allows us to obtain high signal-to-noise ratio in sputter measurements as needed for low ion energies. In most cases, open loop control of the QCM temperature is adequate; for even higher accuracy a closed loop control algorithm is realized in LabView. The criterion used for temperature stability control can be adjusted if necessary to achieve still higher thermal stability, however each measurement takes substantially longer to acquire.

MEASUREMENT PROCEDURES AND DATA ANALYSIS

QCM Measurements and Data Analysis

The angles used to describe the direction of ion incidence and the ejections angles of sputtered particles are shown in Figure 1. The Sauerbrey equation is used to calculate the maximum accumulation rate from the QCM frequency change [6]. At a given measurement point the volumetric differential sputter yield, $y(\alpha,\varphi)$, in units of $mm^3/C/sr$, is determined using Equation (1). Note that because multi-component materials are studied (for which the sputtered particles may comprise various atoms or molecules), volumetric units, e.g., $mm^3/C/sr$ are used, as opposed to atomic based yields, e.g., atoms/ion. In Eqn. (1), $R(\alpha,\varphi)$ is the measured mass accumulation rate (found from the slope of the mass accumulation rate), ρ is the density of target material, $J_{B,avg}$ (C/s) is the time-averaged current of bombarding particles (ions and energetic neutrals) incident on the target, r_{qcm} is the distance from the target center to the QCM (17.4 cm), and A_s is the QCM sensor area (0.535 cm^2).

$$y(\alpha,\phi) = \left[R(\alpha,\phi) r_{qcm}^{\,2} \right] \Big/ \left[\rho J_{B,avg} A_s \right] \qquad (1)$$

In principle, because of the finite size of the QCM crystal and beam spot on the target, each of the measurements (i.e., QCM positions) corresponds to a (small) range of polar and azimuthal angles joining the target and QCM. A simple simulation has been performed to show that for this combination of chamber geometry and sputter conditions these effects are negligible (worst case of 5% error), so that the target and QCM can be treated as points (not areas) joined by a single vector [4]. Experimental uncertainty and error bars on measured differential sputter yields are found by estimating individual contributions and combining them to acquire a value of ± 16%.

As mentioned above, the accuracy and sensitivity of the QCM measurement is ultimately limited by temperature drift and fluctuations, which cause proportional drift and fluctuations of the QCM signal. For high sputter yield materials such as gold, it is found that the signal strength from the QCM is roughly two orders of magnitude larger than the thermal noise. However, for low yield materials, particularly at low ion energies, signal detection is limited by thermal stability. The sensitivity of the QCM allows improvement in the accuracy by at least one order of magnitude beyond present capacity, and work is underway aimed at achieving better thermal stability in the QCM.

As a means to describe the measured differential sputter yield profiles we use expressions from Zhang [7], based on work from Yamamura [8], to which we introduce two fit parameters. We term the resulting expressions as Modified Zhang (MZ) [3]:

$$y_{MZ} = \frac{Y}{1-\sqrt{\frac{E^*}{E}}\cos(\beta)} \cdot \frac{\cos(\alpha)}{\pi}\left[1-\frac{1}{4}\sqrt{\frac{E^*}{E}}\left(\cos(\beta)\gamma(\alpha)+\frac{3}{2}\pi\sin(\beta)\sin(\alpha)\cos(\phi)\right)\right] \quad (2a)$$

$$\gamma(\alpha) = \frac{3\sin(\alpha)^2-1}{\sin(\alpha)^2} + \frac{\cos(\alpha)^2\left(3\sin(\alpha)^2+1\right)}{2\sin(\alpha)^3}\ln\left(\frac{1+\sin(\alpha)}{1-\sin(\alpha)}\right) \quad (2b)$$

where y_{MZ} is the differential sputter yield, Y is the total sputter yield, E is the ion energy, E^* is a characteristic energy describing the profile shape, and the angles are as defined above. The approach decouples the amplitude of the angular profiles from their shape, through the use of Y and E^* respectively. In general, rather than using the MZ expressions for *a priori* calculation, we treat Y and E^* as free fit-parameters which we determine from (least-squares fitting) experimental data. Note that profile shapes are determined by the ratio E^*/E and for high ion energy ($E^*/E << 1$) the MZ expression reduces to the diffuse yield ($y=Y\cos(\alpha)/\pi$). This process is realized by a least-square fitting routine written in Matlab.

Weight Loss Measurement Procedure and Analysis

Sputter yields are also measured using a weight loss method. A microgram-sensitivity scale is used to measure the weight variations from which the volumetric sputter yield, Y (in units of mm^3/C), of each sample is found using Eqn. (3), where Δm represents the mass loss due to ion beam exposure, t is the exposure time, and $J_{B,Avg}$ is the average beam current during the test :

$$Y = \frac{\Delta m}{\rho\, J_{B,Avg}\, t} \quad (3)$$

Measurement uncertainties for total sputter yields are calculated by estimating individual contributions and combining them, yielding an uncertainty of approximately 25%, although this value increases for low-yield materials, as the effects of sources of uncertainty become more dominant.

DEMONSTRATIVE MEASUREMENTS

To illustrate the capabilities of the QCM system, results of testing are presented of a single element target, gold, as well as a multi-element target, boron nitride (BN). The sputter yield of xenon ions on gold was measured at multiple ion energies and angles of incidence, and compared to published data when possible. The total yields from weight loss and QCM (found from the Y parameter of the best-fit MZ profile) were self-consistent to within experimental uncertainty (see Section III). Figure 2a presents the yield versus energy dependence; the data available in the literature are given for comparison. The energy dependence is in good agreement with the Yamamura and Tawara empiric model, except at 30 eV [9]. It should be noted that the threshold sputter energy for xenon ions on gold predicted by Yamamura and Tawara is between 20 and 30 eV, which is in agreement with these measurements – the lowest energy where sputtering was detected was 30 eV. While both this data and Yamamura and Tawara results are consistently higher than Rosenberg and Wehner data, the same trend is observed [7,10].

The angular dependence of the sputter yield of gold is shown in Figure 2b. The sputter yield increases up to an incidence angle

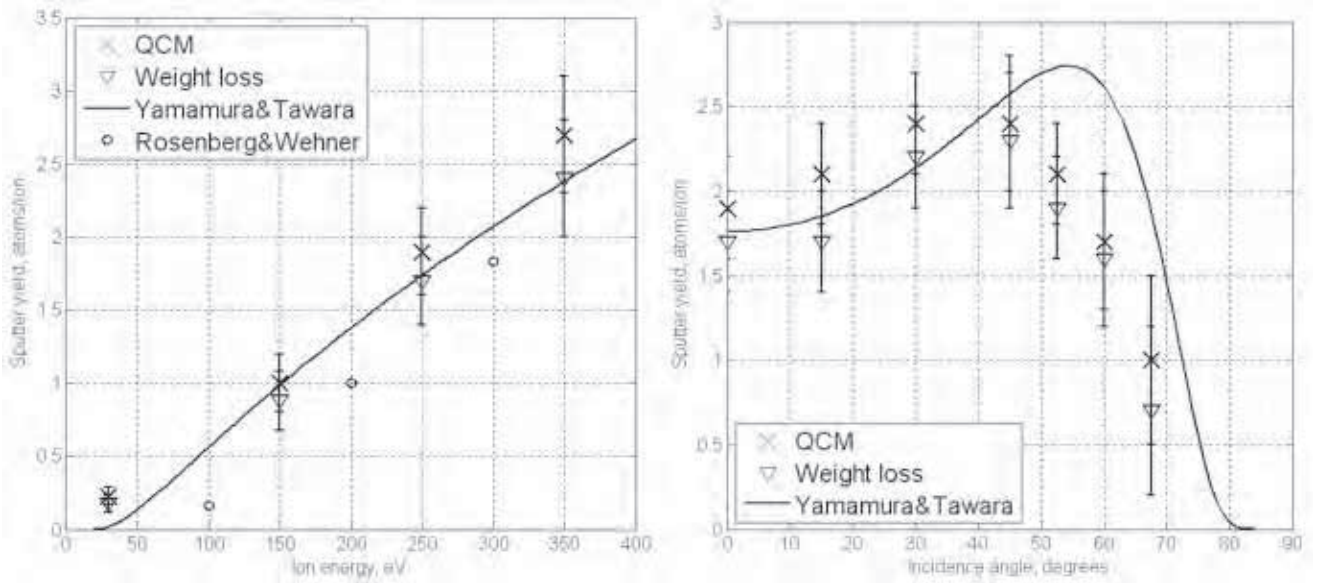

a. *b.*

Figure 2: Xe^+ on Au. Sputter yield versus: a.) ion energy b.) incidence angle.

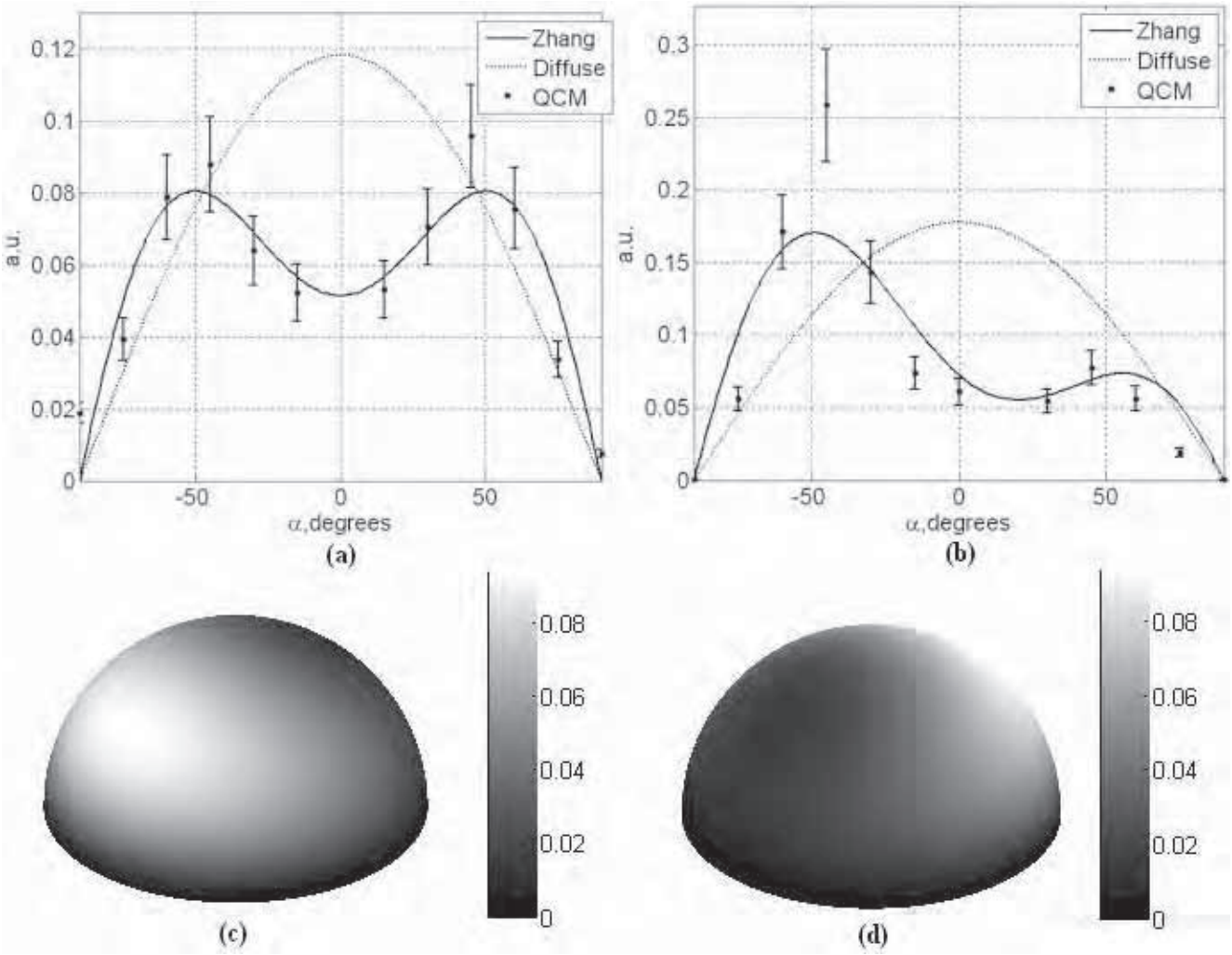

Figure 3: Differential sputter yield, Xe^+ on Au. (a) 350 eV, normal incidence (b) 250 eV, 15 degrees incidence, φ=0 plane. (c) View of forward sputter direction of Zhang-fit hemisphere for 250 eV, β = 30°. (b) View of backward sputter direction.

of 45 degrees before dropping sharply, which is characteristic for most materials. Comparison with Yamamura and Tawara model is also given [9,11]. For angles below 45 degrees the agreement is good, but the model predicts the peak of the angular dependence at slightly higher angle. Still, the character of the angular dependence is in good agreement. Differential sputter yield profiles for 350 eV at normal incidence and for 250 eV at 15 degrees incidence (φ=0 plane) are shown in Figures 3a and 3b. Experimental data and the Zhang fits are shown, and diffuse profiles that correspond to the same sputter yields are given for comparison. For both conditions shown in Figures 3a and 3b, as well as for all other conditions studied in this work, the differential sputter yield profiles were significantly non-diffuse and under-cosine. Figures 3c and 3d show the hemispheric representations of the differential sputter yield calculated from the Modified Zhang equation fitted to the experimental data for an ion energy of 250 eV, and incidence angle of 30 degrees.

To illustrate the capacity of the system with regards to multi-element targets, data taken on BN is presented in Figure 4, below. At low ion energies, BN is thought to sputter predominantly as atomic boron and nitrogen. The QCM measures only condensable particles, in this case boron and possible B_xN_y clusters. The previously mentioned weight loss method can be used to capture the total yield due to all sputtered components. The plots in Figure 4 are of the same nature as those in Figure 3, with (a) and (b) differential sputter yields at 250 eV normal incidence and 30° incidence respectively, while (c) and (d) are the Zhang-fit hemispheres to the data at 250 eV and 30° incidence.

SPUTTER DEPOSITION MODELING

In this section demonstrative modeling that uses the ion beam conditions and differential sputter yield profiles to model and optimize placement of targets and substrates in coating processes is presented. Consider the sputter deposition arrangement shown in Figure 5a. A 500 mA, 250 eV xenon ion

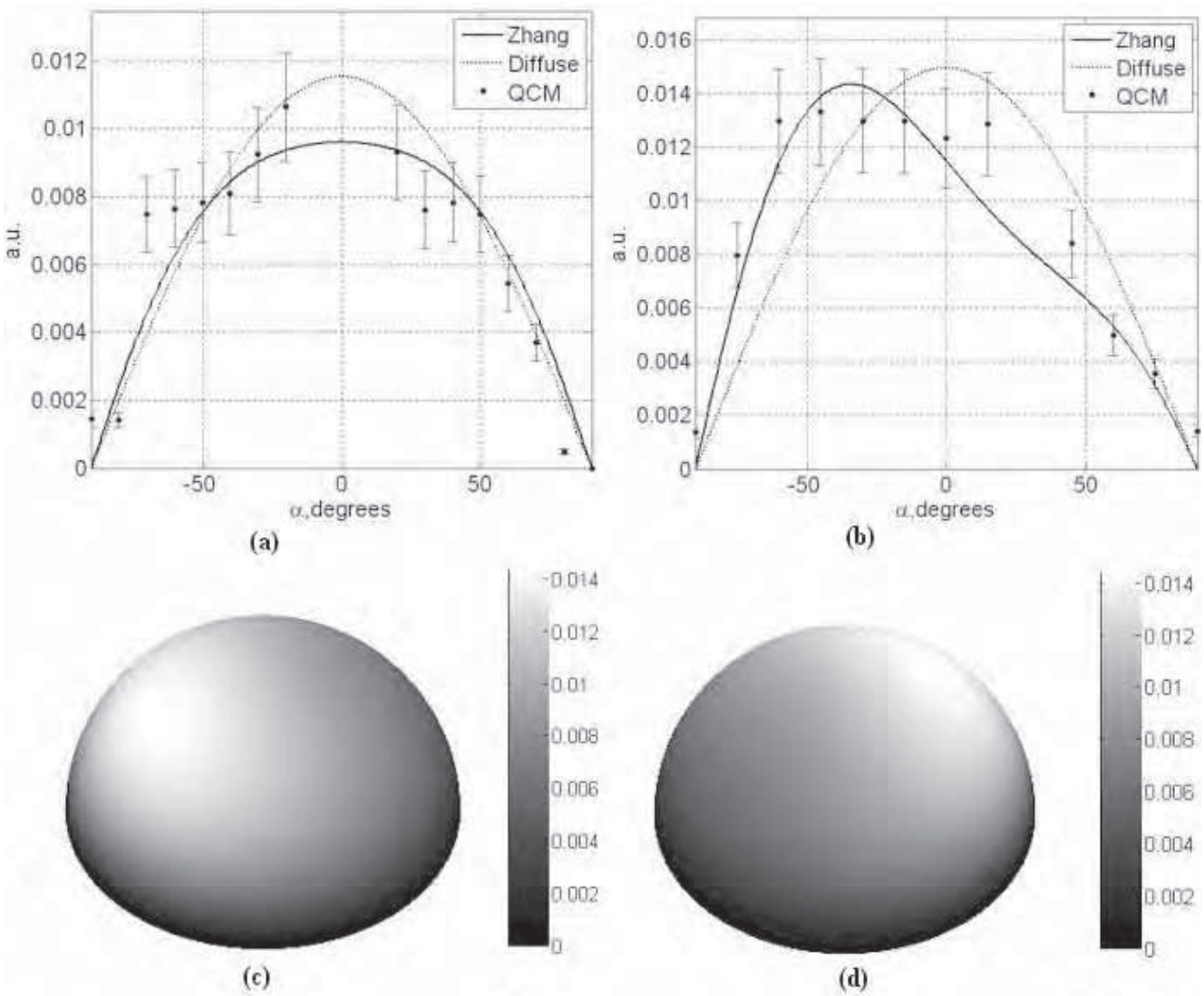

Figure 4: Differential sputter yield, Xe^+ on BN. a.) 250 eV, normal incidence b.) 250 eV, 15 degrees incidence, φ=0 plane. c.) View of forward sputter direction of Zhang-fit hemisphere for 250 eV, β = 30°. d.) View of backward sputter direction.

beam emanates from a 5 cm diameter source and strikes a 15 cm diameter gold target, which is large enough such that all of the ion beam current is collected on the target. The cosine and Zhang differential sputter yield models were used to calculate the flux (atoms/m^2s) of sputtered gold atoms to an 8 cm diameter substrate. The angle between the ion beam and target normal, β, was varied from 0° to 60°. The total fluxes were integrated over the substrate area, and the results are listed in Figure 5b. The fluxes were normalized to the result at β = 0° of $1.51 \cdot 10^{17}$ atoms/s, calculated using the Zhang model. For this test setup, the cosine model leads to overestimations of the atomic flux and deposition rate, values for which vary from 6 to 44%. A visualization of the atomic flux using the cosine and Zhang models is shown in Figures 5c and 5d for the case where β = 15°.

CONCLUSIONS

The QCM based system used for total and differential sputter yield measurements at this facility has been described. The ion source and detection system allow high sensitivity for measurements over a range of ion energies and sputter conditions. Demonstrative measurements and sputter modeling have been presented.

ACKNOWLEDGMENTS

The authors would like to thank Loral Space Systems for funding support. The authors also thank Paul Wilbur and John Williams (Colorado State University) for assistance and initial development of the QCM apparatus.

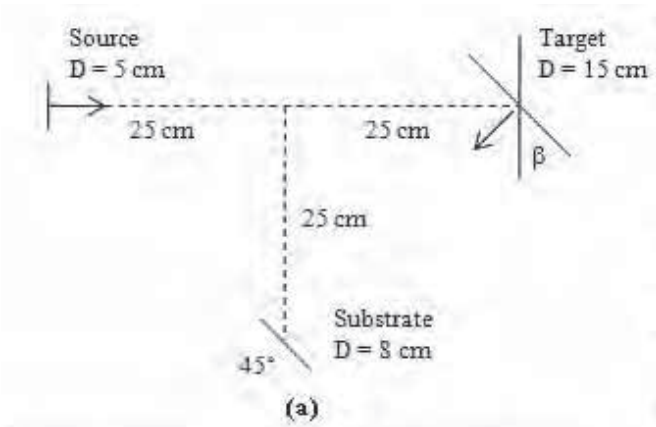

(a)

Angle β (°)	Atom Influx - Zhang	Atom Influx - Cosine	Relative Error (%)
0	1.00	1.05	5.5
15	1.19	1.28	7.2
30	1.50	1.82	21.4
45	1.35	1.95	44.3
60	0.91	1.29	41.5

(b)

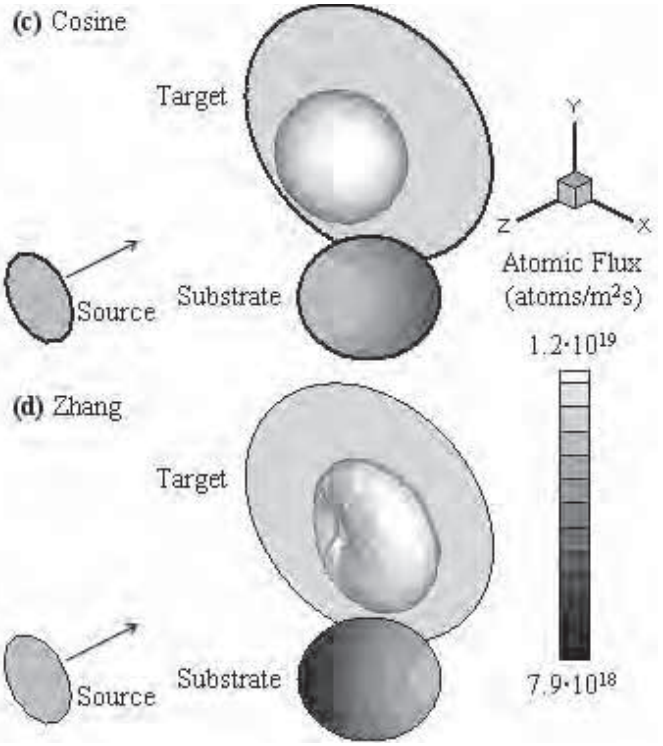

Figure 5: a.) Numerical test case setup. b.) Atomic flux to the substrate using Zhang and cosine emission models, normalized. c.) Visualization of atomic flux from target to substrate, β=15°, cosine model and d.) Zhang model.

REFERENCES

1. G. Betz and K. Wien "Energy and angular distributions of sputtered particles," *Int. J. Mass Spectrom. Ion Processes*, 140 1-110, 1994

2. K.A. Zoerb, J.D. Williams, D.D. Williams, and A. P. Yalin "Differential sputtering yields of refractory metals by xenon, krypton, and argon ion bombardment at normal and oblique incidences," 29th *International Electric Propulsion Conference (Princeton, NJ)*, IEPC-2005-293, 2005

3. A.P. Yalin, J.D. Williams, V. Surla, and K.A. Zoerb, "Differential Sputter Yield Profiles of Molybdenum due to Bombardment by Low Energy Xenon Ions at Normal and Oblique Incidence," *J. Phys. D: Appl. Phys.* 40 3194-3202, 2007

4. B. Rubin, J. Topper, and A.P. Yalin, "QCM Based System for High-Sensitivity Differential Sputter Yield Measurements," manuscript in preparation

5. L. Bachmann, and J.J. Shin, "Measurement of the Sticking Coefficients of Silver and Gold in an Ultrahigh Vacuum," *J. Appl. Phys.*, Vol. 37, No. 1, pp. 242-246, 1966

6. P. Sigmund, "Theory of sputtering I: sputtering yield of amorphous and polycrystalline targets," *Phys. Rev.* 184 383-416, 1969

7. Z.L. Zhang, and L. Zhang, "Anisotropic angular distributions of sputtered atoms" *Rad. Eff. Def. Sol.* 159 301-07, 2004

8. Y. Yamamura, "Theory of sputtering and comparison to experimental data," *Nucl. Instr. and Meth.* 194 515–22, 1982

9. Y. Yamamura, and H. Tawara, "Energy Dependence of Ion-Induced Sputtering Yields from Monatomic Solids at Normal Incidence," *At. Data Nucl. Data Tables*, Vol 62, No. 2, pp. 149-253, 1996

10. G.K. Wehner and D. Rosenberg, "Angular Distribution of Sputtered Material," *J. Appl. Phys.* 31 177-9, 1960

11. Y. Yamamura, Y. Itikawa, and N. Itoh, "Angular Dependence of Sputtering Yields of Monatomic Solids," *Institute for Plasma Physics Report* IPPJ AM-26, 1983.